Competing itinerant and localized states in strongly correlated $BaVS_3$

Frank Lechermann,[1] Silke Biermann,[2] and Antoine Georges[2]
[1]*I. Institut für Theoretische Physik, Universität Hamburg, D-20355 Hamburg, Germany*
[2]*CPHT, École Polytechnique, 91128 Palaiseau Cedex, France*
(Received 19 April 2007; published 2 August 2007)

The electronic structure of the quasi-low-dimensional vanadium sulfide $BaVS_3$ is investigated for the different phases above the magnetic ordering temperature. By means of density functional theory and its combination with dynamical mean-field theory, we follow the evolution of the relevant low-energy electronic states on cooling. Hence, we go in the metallic regime from the room temperature hexagonal phase to the orthorhombic phase after the first structural transition and close with the monoclinic insulating phase below the metal-insulator transition. Due to the low symmetry and expected intersite correlations, the latter phase is treated within cellular dynamical mean-field theory. It is generally discussed how the intriguing interplay between band-structure and strong-correlation effects leads to the stabilization of the various electronic phases with decreasing temperature.

DOI: 10.1103/PhysRevB.76.085101 PACS number(s): 71.30.+h, 71.15.Mb, 71.10.Fd, 75.30.Cr

I. INTRODUCTION

Since its first characterization[1] in 1969, the understanding of the complex electronic structure of the vanadium sulfide $BaVS_3$ poses a long-standing problem in condensed matter physics.[2–6] Numerous experimental and theoretical studies have revealed a delicate coupling between orbital, spin, and lattice degrees of freedom over a wide temperature range. On cooling, $BaVS_3$ exhibits three continuous phase transitions, starting with a structural hexagonal-to-orthorhombic transition at $T_S \sim 240$ K in the metallic regime. The latter vanishes at ~ 70 K where a metal-to-insulator transition (MIT), accompanied by a lattice transformation from orthorhombic to monoclinic,[7,8] to a still paramagnetic phase takes place. A final magnetic transition marking the onset of an incommensurable antiferromagnetic order[9,10] sets in at $T_X \sim 30$ K.

The underlying driving forces for these transitions and the specific nature of the respective phases are to a large extent still a matter of debate. It was shown[11] that the MIT may be driven to zero temperature at high pressure, and the suppression of the insulating phase leads to non-Fermi-liquid and quantum-critical behavior.[12] This observation does not only add even more complexity to the already existing problems but also underlines the tricky nature of the electronic structure. At ambient pressure, the MIT is announced early by strong precursive behavior such as a large increase of the Hall coefficient[5] and a wide one-dimensional (1D) lattice-fluctuation regime[13] along the c axis of the system. In fact, it seems to be established[7,8,13,14] that the MIT may be described in terms of a charge-density wave (CDW) instability. However, $BaVS_3$ is not a textbook Peierls system. The dc conduction anisotropy is rather small[15] ($\sigma_c/\sigma_a \sim 3$–4), and the "metallic" phase above T_{MIT} displays a high resistivity (a few mΩ cm) and metallicelike behavior ($d\rho/dT > 0$) only above a weak minimum at ~ 150 K, below which it increases upon further cooling.[4,15] Moreover, local-moment behavior is revealed from the magnetic susceptibility, with an effective moment of approximately one localized spin 1/2 per two V sites. At T_{MIT}, the susceptibility rapidly drops, and the electronic entropy is strongly suppressed.[16]

Because of the nominal V^{4+} valence, $BaVS_3$ belongs to the family of $3d^1$ compounds with a t_{2g} manifold spanning the low-energy sector. In the hexagonal phase, the latter consists (per V ion) of an A_{1g} and two degenerate E_g states. The remaining e_g states are strongly hybridized with the S($3p$) states and have major high-energy weight. Below T_S, the degeneracy of the E_g states is lifted in the orthorhombic phase. In both phases, the primitive cell includes 2 f.u., where the V and S ions form chains of face-sharing VS_3 octahedra along the c axis. The intrachain V-V distance is less than half the interchain distance. It follows[2] that the A_{1g} orbital is mainly directed along the chain, forming a broader band due to the significant overlap of neighboring intrachain V ions. On the contrary, the lobes of the E_g orbitals point in between the sulfur ions, i.e., do not hybridize strongly with their environment, leading to comparably narrow bands. These simple characterizations hold essentially also for the monoclinic insulating phase, yet the primitive cell is doubled and the resulting four V ions in the basis are now all inequivalent by symmetry.[8,17] The CDW mechanism has led to a tetramerization, yet no evident charge disproportionation among them was detected.[17] The measured charge gap[4,15,18,19] of about 40 meV is twice as large as the apparent spin gap,[20] pointing once more toward the relevance of electronic correlations.[21]

In Refs. 14 and 22, the orthorhombic phase above the MIT was investigated, and it was argued that strong electronic correlations are responsible for a substantial charge transfer within the t_{2g} states, leading also to important Fermi-surface changes in comparison to a weak-correlation treatment. Here, we go further by tracing the low-energy states of $BaVS_3$ all the way from room temperature down to 40 K (just above the final magnetic transition). Although the local environment of the V site does not change dramatically, the electronic structure appears to be rather sensitive to the temperature changes. This originates from the subtle balance of kinetic energy versus Coulomb interaction in the electronic system, a characteristic of strongly correlated materials. In fact, this vanadium sulfide presents an interesting realistic realization of one of the basic problems in strongly corre-

 ©2007 The American Physical Society

lated physics: There is nominally one electron in the low-energy sector and two distinct orbital states, one forming a broader band and two forming narrower bands. Hence, depending on temperature, nature shall find the best compromise between kinetic energy gain and potential cost due to mutual Coulomb interaction in this multiorbital scenario.

II. THEORETICAL FRAMEWORK

For the investigation of competing band-structure and many-body effects in realistic materials, the combination[23,24] of density functional theory (DFT) and dynamical mean-field theory (DMFT) has recently proven to be a powerful approach.

For the DFT part, we used the local density approximation (LDA) to the exchange-correlation energy. The corresponding calculations were performed with a mixed-basis pseudopotential code.[25] It uses norm conserving pseudopotentials and plane waves supplemented with some few nonoverlapping localized functions in order to represent the pseudocrystal wave function.

Since the low-energy physics of $BaVS_3$ is dominated by the t_{2g} states, the so-called LDA+DMFT calculations were performed for the corresponding three-band subset. The latter was derived from the full band structure via the maximally localized Wannier function (MLWF) construction.[26,27] Hence, the local orbitals which form the impurity in the DMFT context stem from the associated Wannier functions (WFs) and the low-energy LDA Hamiltonian $H(\mathbf{k})$ is expressed with respect to these orbitals.[14] To be specific, by making reference to the formalism outlined in Ref. 14, in all LDA+DMFT calculations presented here, the set of correlated orbitals $\mathcal{C}$ was identical to the set $\mathcal{W}$ of the WFs forming the minimal LDA Hamiltonian. Hence, the impurity Green's function is computed in DMFT for finite inverse temperature β via

$$\mathbf{G}(i\omega_n) = \sum_{\mathbf{k}} [(i\omega_n + \mu)\mathbb{1} - H^{(\mathcal{C})}(\mathbf{k}) - \mathbf{\Sigma}^{(\mathcal{C})}(i\omega_n)]^{-1}, \quad (1)$$

where $\omega_n = (2n+1)\pi/\beta$ are the Matsubara frequencies and $\mathbf{\Sigma}$ is the self-energy matrix for the strongly correlated orbitals. For the local interacting Hamiltonian H_{int}, the following representation restricted to density-density terms only was used:

$$\hat{H}_{\text{int}} = U\sum_{m} \hat{n}_{m\uparrow}\hat{n}_{m\downarrow} + \frac{U'}{2}\sum_{\substack{mm'\sigma \\ m\neq m'}} \hat{n}_{m\sigma}\hat{n}_{m'\bar{\sigma}} + \frac{U''}{2}\sum_{\substack{mm'\sigma \\ m\neq m'}} \hat{n}_{m\sigma}\hat{n}_{m'\sigma}. \quad (2)$$

Here, $\hat{n}_{m\sigma} = \hat{d}^{\dagger}_{m\sigma}\hat{d}_{m\sigma}$, where m, σ denote orbital and spin indices. The following parametrization of U' and U'' has been proven to be reliable[28,29] in the case of t_{2g}-based systems: $U' = U - 2J$ and $U'' = U - 3J$. We utilized the quantum Monte Carlo (QMC) formalism after Hirsch-Fye[30] to solve the impurity problem.

For hexagonal and orthorhombic $BaVS_3$, there are only symmetry-equivalent V ions in the primitive cell and, moreover, interatomic correlation effects are not expected to be of crucial importance. Hence, a single-site DMFT approach to describe the strong-correlation effects was employed for those phases. Thereby, the inverse temperature was always $\beta = 30\ \text{eV}^{-1}$ and the number of time slices equaled 128 for the QMC method. However, since the paramagnetic insulating regime of the low-temperature monoclinic phase is associated with a CDW state, this approximation appears inadequate. We thus used a cluster formalism (for recent reviews see, e.g.. Refs. 31–33), namely, the cellular DMFT (CDMFT) approach in a realistic context.[33,34] More explicitly, the linear cluster formed by the four symmetry-inequivalent V ions, each one decorated with a three-orbital t_{2g} multiplet, was identified as the impurity for the CDMFT scheme. This amounts to a self-energy matrix $\mathbf{\Sigma}(i\omega_n)$ that is off-diagonal not only in the orbital indices but also in the site indices within the cluster. Note, however, that intercluster components of the self-energy are neglected. The latter fact results in the breaking of translational symmetry when computing pair correlations for the end sites of our linear cluster. However, such a cluster approach should still be sufficient to describe the major qualitative changes in the correlated electronic structure originating from the CDW instability. Since the undertaken cluster investigation is numerically very expensive within QMC (to our knowledge one of the largest up to now performed in the framework of realistic cluster DMFT), we chose $\beta = 25\ \text{eV}^{-1}$ and used 90 time slices.

TABLE I. Experimental crystal data used for the investigation of $BaVS_3$.

	RT	100 K	40 K
Crystal system	Hexagonal	Orthorhombic	Monoclinic
Space group	$P6_3/mmc$	$Cmc2_1$	Im
a (a.u.)	12.71	12.77	12.78
b (a.u.)	22.01($=a\sqrt{3}$)	21.71	21.65
c (a.u.)	10.63	10.58	21.15
β (deg)			90.045
Experiment	Ref. 36	Ref. 36	Ref. 8

III. RESULTS

Stoichiometric $BaVS_3$ transforms on cooling successively to crystal systems with lower symmetry, giving a hint to the generally low ordering energy. Table I summarizes the basic crystal data for the three different phases that are studied in this work. Both the hexagonal and orthorhombic phases are associated with the metallic regime, while the monoclinic phase corresponds to the insulating system. Here, we only investigated the paramagnetic phase of the insulator and excluded the magnetically ordered phase below T_X.

A. LDA study of the metallic regime

At room temperature (RT), $BaVS_3$ crystallizes in the hexagonal ($P6_3/mmc$) structure[1] with 2 f.u. in the primitive cell. All symmetry operations of the hexagonal group apply to this structure, and all Ba, V, and S ions in the cell form one single symmetry class, respectively. The V ions within the

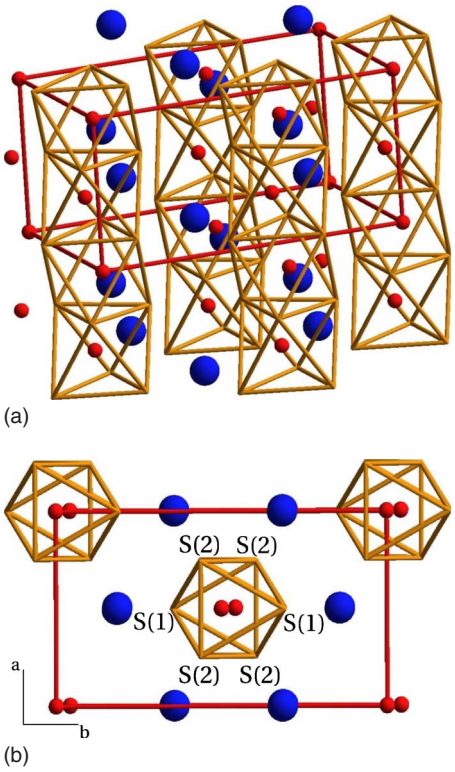

FIG. 1. (Color online) $BaVS_3$ in the $Cmc2_1$ structure. The V ions are shown as smaller (red/gray) spheres and the Ba ions as larger (blue/dark) spheres.

chains are aligned straightly. As noted by Mattheiss,[37] the variable parameter x(S) which determines the in-plane S-S distances deviates slightly from the ideal hexagonal value, i.e., $x(\mathrm{S})=0.1656$ while $x_{\mathrm{ideal}}=1/6$. This means that the in-plane equilateral S-S-S triangle above and below a V ion is contracted and the intrachain S-S bond lengths are decreased in comparison to the interchain lengths.

At T_S, the crystal system transforms from hexagonal to orthorhombic, leading to a structure with ($Cmc2_1$) space group. The V chains are now zigzag distorted in the bc plane of the lattice. Although still 2 f.u. form the primitive cell, the symmetry class of the sulfur ions has split into two: both S1 ions are positioned at (4a) apical sites on the b axis, while the four S2 ions occupy (8b) sites (see Fig. 1). From Table I, it is seen that the structural transformation results in only minor changes in the lattice parameters, with a maximum of 1.5% contraction of the b axis. There are several LDA studies for $BaVS_3$ above the MIT.[18,22,37,38] In addition to those, a direct comparison of the LDA low-energy electronic structure for the hexagonal and orthorhombic phases via Wannier construction for the t_{2g} manifold is presented here.

Figure 2 displays the LDA density of states (DOS) for the two crystal structures. In each case, the dominance of the t_{2g} states at low energy, with a prominent peak right at the Fermi energy, is evident. For the A_{1g} band, the dispersion is indeed reminiscent of 1D characteristics; however, below the Fermi energy, features are changed due to hybridization with the $S(3p)$ states. The weight of the latter states is reduced in the energy range $[-1,0]$ for the $Cmc2_1$ structure compared to the $P6_3/mmc$ structure. One might interpret this as some decoupling of A_{1g} and $S(3p)$ throughout the structural transition. The very large DOS at the Fermi energy, common to both structures, due to the E_g states render instabilities towards broken-symmetry phases very likely.

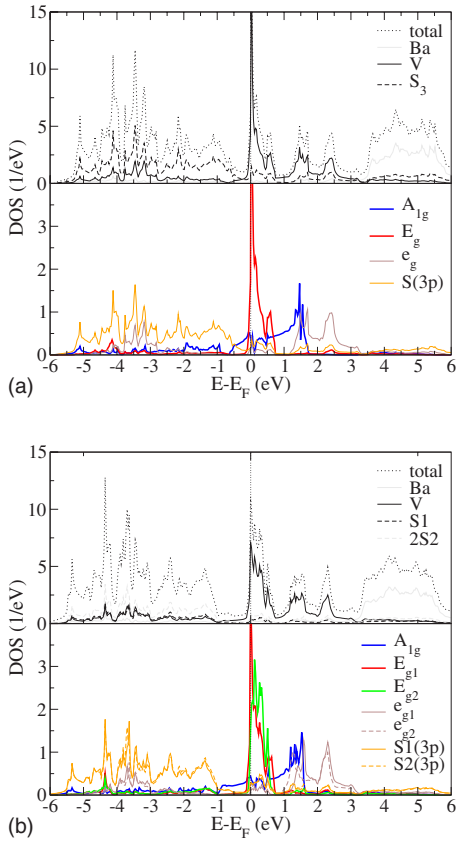

FIG. 2. (Color online) Total and local LDA DOS for $BaVS_3$ in (a) the $P6_3/mmc$ structure and (b) the $Cmc2_1$ structure.

The LDA band structures in Figs. 3 and 4, with "fat bands" exhibiting the weight of the respective t_{2g} states on the different bands,[14] show the folded character of the A_{1g}

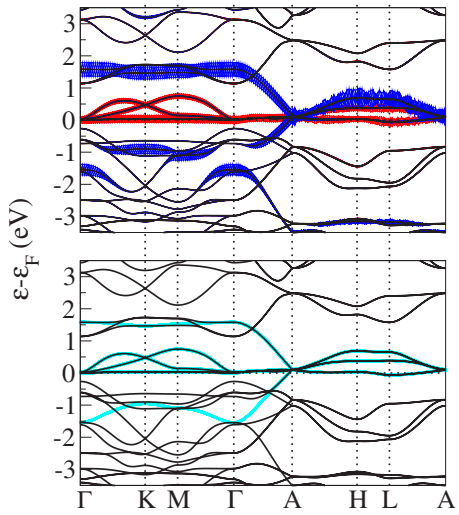

FIG. 3. (Color online) (Top) LDA band structure and (bottom) derived t_{2g} Wannier bands for $P6_3/mmc$ $BaVS_3$. Color coding for (top): A_{1g} (blue/dark) and E_{g1}/E_{g2} (red/gray).

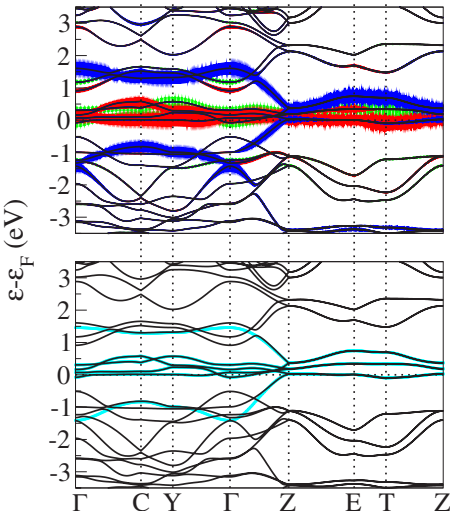

FIG. 4. (Color online) (Top) LDA band structure and (bottom) derived t_{2g} Wannier bands for $Cmc2_1$ $BaVS_3$. Color coding for (top): A_{1g} (blue), E_{g1} (red), and E_{g2} (green).

band due to the 2 f.u. primitive cell. The A_{1g} bandwidth is dominated by the dispersion along Γ-(A,Z), i.e., along the c^* axis. While for the higher-symmetry $P6_3/mmc$ structure the folding propagates gapless through A, the corresponding bands are separated at Z for the $Cmc2_1$ structure. This hybridization between A_{1g} and E_g is obvious in the upper triangles A-H-L and Z-E-T. Clearly seen is the hybridization of A_{1g} with $S(3p)$ resulting in "jumps" of the A_{1g} character between different bands in the lower triangles Γ-K-M and Γ-C-Y. For both structures, the A_{1g} band cuts the Fermi level ε_F close to the zone boundary, leading to a nearly filled lower part of the folded band complex. It was noted in former works[3,6] that for $Cmc2_1$, this filling renders a CDW instability within the A_{1g} band along Γ-Z impossible.

The E_g states form very narrow, in some regions even nearly dispersionless, bands right at ε_F. An important difference occurs between the Fermi surface (FS) of the two metallic phases (see Fig. 5). Although in both cases the FS consists of two sheets, the one for $P6_3/mmc$ is entirely located at the zone boundaries with a dominant A_{1g} sheet and smaller E_g pockets around L. On the contrary, the FS for $Cmc2_1$ shows as the first sheet a substantial E_{g2} electron pocket centered at Γ and E_{g1} pillarlike structures on the b^* axis extending along c^*. The FS is completed by the A_{1g} sheet, now extending deeper into the Brillouin zone (BZ). Despite the latter observation, this quasi-1D sheet is neither strongly flattened nor have both parts the proper distance for nesting with the experimental CDW vector $[\mathbf{q}_c^{(\mathrm{exp})}=0.5\mathbf{c}^*]$.

The dispersions according to the derived three-band Hamiltonian on the basis of the maximally localized procedure[26,27] are shown in Figs. 3 and 4. Because of the entanglement of the V($3d$) bands with the $S(3p)$ ones, the dominant A_{1g}-like band does not coincide with the true LDA bands in this minimal model.[14] Still, such a three-band approach should carry the essential physics in the low-energy regime. Figure 6 pictures the corresponding V(t_{2g}) Wannier orbitals in the crystal-field basis, i.e., with vanishing on site hybridization. For both phases, it is seen that the E_{g1} orbitals

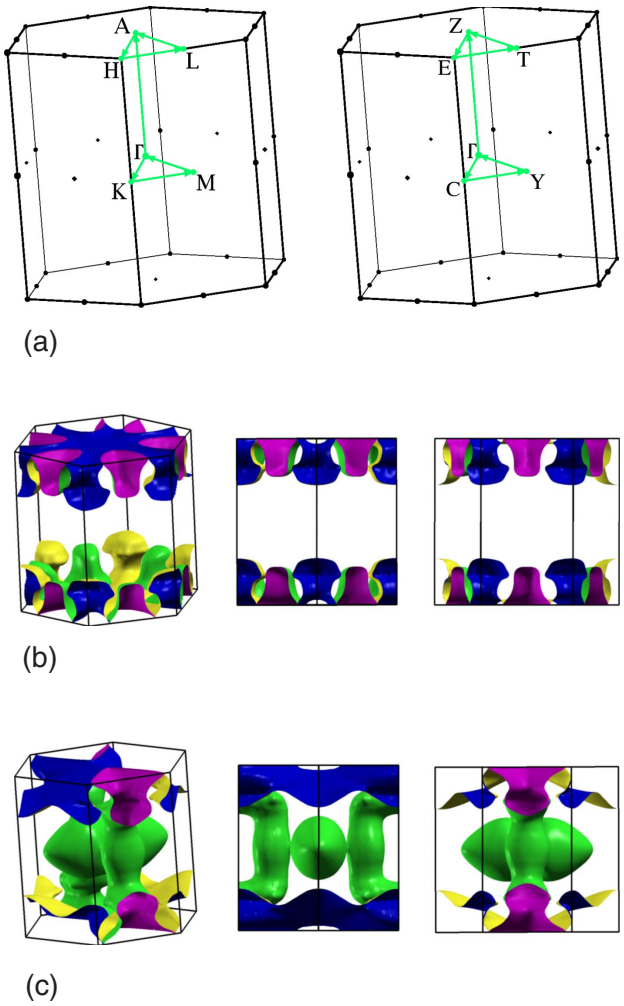

FIG. 5. (Color online) (a) Hexagonal and orthorhombic Brillouin zones, as well as LDA Fermi surface for $BaVS_3$ in (b) the $P6_3/mmc$ structure and (c) the $Cmc2_1$ structure from different perspectives.

leak out on the S2 ions, while the E_{g2} orbitals have weight on the apical S1 atoms [recall that (S1,S2) are symmetrically equivalent only in the hexagonal phase]. The A_{1g} orbital hybridizes with the $3p$ orbitals on both sulfur-ion types. That this hybridization is indeed weakened in the $Cmc2_1$ structure may be derived from the reduced spread of the A_{1g} WF shown in Table II. Interestingly, the spread is now even below the values for the E_g states. Note also that the WF centers are identical with the V positions only for the hexagonal structure, while there are some shifts for the orthorhombic structure. The main qualitative difference in the hopping integrals (Table III) between the two structures is the emerging substantial hybridization between A_{1g} and E_{g1} for $Cmc2_1$. Note that, generally, the E_g hoppings are rather isotropic, whereas the dominating hopping along the c axis in the case of A_{1g} is obvious.

B. LDA+DMFT study of the metallic regime

The LDA approach presented in the previous section underlies the assumption that the mutual interactions between

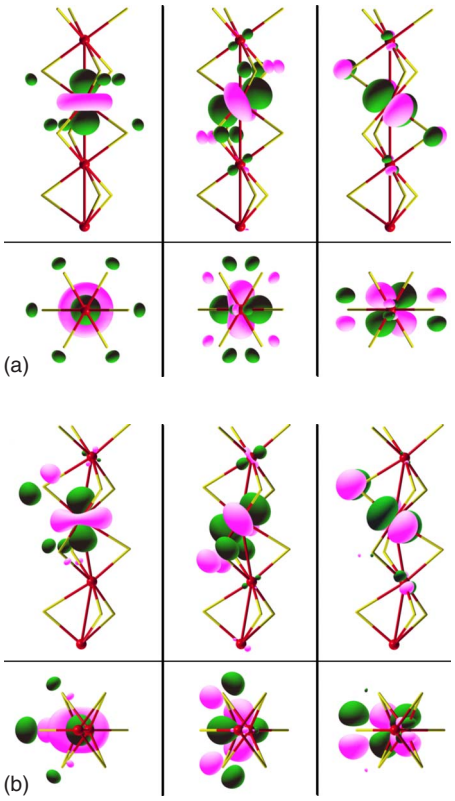

FIG. 6. (Color online) t_{2g} Wannier functions for $BaVS_3$ in the crystal-field basis of (a) the $P6_3/mmc$ structure and (b) the $Cmc2_1$ structure.

the electrons may be cast into a static local exchange-correlation potential within an effective single-particle description. However, it is known that for strongly correlated systems, such a description is likely to fail. Since one indeed expects rather strong correlations within the quarter-filled $V(t_{2g})$ states of $BaVS_3$, also due to the specific characteristics of very narrow E_g bands and the broader A_{1g} band, we employed the LDA+DMFT framework to explicitly include many-body effects in the electronic structure.

TABLE II. Wannier centers $\mathbf{R}_w$ and spread $\langle r^2 \rangle$ of the t_{2g}-like MLWFs constructed from a $(6\times6\times6)$ k-point mesh. The positions of the symmetrically equivalent V sites in Cartesian coordinates (in a.u.) for $P6_3/mmc$ read as follows: $\mathbf{R}_{V1}=(0.00,0.00,0.00)$ and $\mathbf{R}_{V2}=(0.00,0.00,5.30)$. For $Cmc2_1$, they are as follows: $\mathbf{R}_{V1}=(0.00,0.46,-0.01)$ and $\mathbf{R}_{V2}=(0.00,-0.46,5.28)$. The V(2) site is symmetry related to the V(1) site by the symmetry operation $C_2^{(z)}\mathbf{R}_{V1}+0.5$. In the following, only the data for V1 are shown.

Structure	WF	$\mathbf{R}_w-\mathbf{R}_{V1}$ (a.u.)	$\langle r^2 \rangle$ (a.u.^{2})
$P6_3/mmc$	A_{1g}	0.00, 0.00, 0.00	18.62
	E_{g1}	0.00, 0.00, 0.00	17.10
	E_{g2}	0.00, 0.00, 0.00	17.10
$Cmc2_1$	A_{1g}	0.00, 0.30, −0.16	16.60
	E_{g1}	0.00, 0.19, 0.35	17.55
	E_{g2}	0.00, 0.56, −0.31	17.53

By identifying the derived t_{2g} WFs in the crystal-field basis as the subspace of correlated orbitals, we obtained the **k**-integrated (local) spectral functions $\rho(\omega)$ shown in Fig. 7. Clearly seen is the transfer of spectral weight from the quasiparticle (QP) peaks to lower or higher energies in comparison to the local LDA DOS, especially for the E_g states. This corresponds to an inclusion of the atomiclike excitations important for states with substantial localized character, which is missing in the standard LDA picture. By varying T, one observes[22] additionally that the strength of the E_g QP peak changes also more significantly. Thus, the corresponding electrons are effectively localized for a wide temperature range due to incoherence effects.

Since the correlation effects influence the subtle energetic balance in this system, they are moreover responsible for a substantial charge transfer between the relevant orbitals,[14,22] resulting in different orbital-resolved fillings compared to the LDA ones (see Table IV). The LDA filling of the A_{1g} band is close to 70% in the hexagonal structure and does not change much for temperatures where the DMFT study was elaborated. A reasonable choice[22] for the Hubbard parameters U and J leads to a significant transfer of charge from A_{1g} to E_g, in order to overcome the large potential energy cost for occupying mainly the former orbital. The new fillings for E_{g1} and E_{g2} differ slightly due to a marginal hybridization between A_{1g} and E_{g1} in the Wannier Hamiltonian already for the hexagonal structure. Note that *filling* in LDA+DMFT is not equivalent to pure band filling in the LDA sense, because the atomiclike excitations are now also included. The essential change for the orthorhombic structure below T_S (which was treated here at the same T within the QMC solver of DMFT) is the effective reduction of the three-band to a dominant two-band problem. Due to the now substantial A_{1g}-E_{g1} hybridization, the charge transfer is dominantly taking place between those two orbitals. Yet the overall occupation of the A_{1g} orbital is only a little smaller than in the hexagonal phase. The E_{g1} filling is now close to 50%, in good agreement with the experimentally observed local magnetic moment of about one free spin every other V ion.

Besides the orbital-resolved filling, the change of the respective FS sheets in the metallic regime is also of large interest. However, keep in mind that there is no straightforward relation between those two issues, as only the *total* Fermi-surface volume is invariant when turning on correlations and no unique rule on how the individual sheets have to change can be derived. However, this change can of course be calculated, which was done for the orthorhombic phase with the Wannier basis in Ref. 14, and the change of the FS sheets is indeed in line with what one expects from the overall charge transfers (see Fig. 8). More explicitly, a strong Fermi-surface deformation was revealed, placing parts of the renormalized A_{1g} sheet now in reasonably good position for a possible nesting with the experimentally determined **q** vector. An important observation was that the nesting should mainly take place away from the high-symmetry directions in the BZ, i.e., the A_{1g} band along the Γ-Z direction should not be strongly involved in the direct nesting. As pointed out, one expects the E_g states to be essentially localized for higher temperatures, rendering the definition of a sharp FS rather difficult. For this reason, no renormalized FS was

TABLE III. Hopping integrals between the t_{2g} Wannier orbitals of $BaVS_3$ in the crystal-field basis. The first value corresponds to the $P6_3/mmc$ structure and the second to the $Cmc2_1$ structure, respectively. The term "$00\frac{1}{2}$" shall denote the hopping to the nearest-neighbor V site within the unit cell. One of the nearest-neighbor V ions in the *ab* plane is located at "100," while "110" and "$\bar{1}10$" are closest V ions along *a* and *b*, respectively. Energies are in meV.

	A_{1g}	A_{1g}	E_{g1}	E_{g1}	E_{g2}	E_{g2}	A_{1g}	E_{g1}	A_{1g}	E_{g2}	E_{g1}	E_{g2}
000	395	423	200	210	200	236	0	0	0	0	0	0
$00\frac{1}{2}$	−587	−511	90	44	−90	−12	0	−146	0	0	0	0
001	−61	−86	5	14	5	3	0	7	0	0	0	0
100	−49	−35	8	14	−40	−26	18	−7	−32	−14	41	14
110	−49	−26	−63	−76	31	29	−37	−28	0	−2	0	−12
$\bar{1}10$	3	1	0	2	−5	−6	0	−2	0	0	0	0

computed for the hexagonal phase. Due to the missing A_{1g}-E_{g1} hybridization, one would, however, expect that for this phase, the overall A_{1g} sheet is shifted more or less coherently in the BZ, contrary to the orthorhombic case.

C. LDA study of the paramagnetic insulating regime

$BaVS_3$ below T_{MIT} is insulating with a monoclinic *Im* structure involving 4 f.u. in the primitive cell.[8] The system is described as a CDW state with a dominant $2k_F$ distortion.[8] Figure 9 displays the four inequivalent vanadium ions along the chain, together with numbers indicating the shift of the atomic positions with reference to the $Cmc2_1$ structure above the MIT (at $T=100$ K). It is seen that the shifts for V along the chain are relatively small, on the scale of 4% at most. Nonetheless, a dominant distortion pattern for this CDW state may be identified. The mainly shifted ions are V1 and V3 in our notation, whereas V2 and V4 only marginally change their positions. Since V1 and V3 are shifted toward each other, with V4 in between, the tetramerization appears as an effective trimerization, isolating the V2 site. As a result, the V-V distances in decreasing order are: V2-V3, V1-V2, V1-V4, and V3-V4. To a smaller extent, the average V-S distance (taking into account only the six nearest-neighbor sulfur ions, respectively) also varies. Again, the averaged distance $\Delta\bar{d}_{VS}$ is largest for the V2 ion and smallest for the V4 ion.

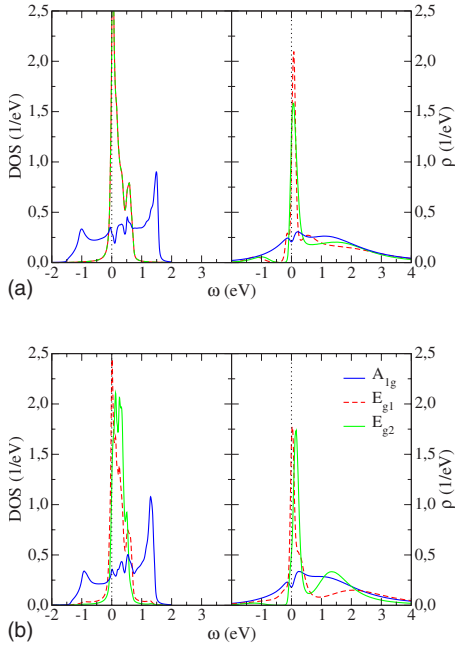

FIG. 7. (Color online) (Right) Local spectral functions from LDA+DMFT in comparison to (left) the local LDA DOS for the t_{2g} WFs in the crystal-field basis for (a) the $P6_3/mmc$ structure and (b) the $Cmc2_1$ structure. The QMC solver was used for $T=390$ K.

Although the CDW phase is experimentally known[4] to be paramagnetic insulating, the LDA calculation finds it to be metallic (see Fig. 10). Hence, whereas the insufficiency of LDA for the metallic regime required a closer band-structure study, the failure due to the neglection of strong correlations is now obvious. Still, the LDA approach may deliver relevant information about the kinetic part of the Hamiltonian and the changes of the electronic structure due to the CDW distortion.

The total LDA DOS for the *Im* structure is rather close to the $Cmc2_1$ one. We plotted in Fig. 10 only the Wannier bands for the low-energy regime on top of the full LDA band structure. The lowest and highest t_{2g} bands still have the strongest A_{1g} weight, and the hybridization between A_{1g} and E_{g1} is significant especially at higher energy. However no clear distinction between the individual electronic characters of the V ions can be made on the level of simple projection onto local orbitals.

A bit more insight is obtained when going to the Wannier representation, again using the crystal-field basis as the choice of reference. Figure 11 indicates that from a low-

TABLE IV. Orbital-resolved fillings for $BaVS_3$ from LDA+DMFT within the crystal-field Wannier basis. The QMC solver was used for $T=390$ K.

Structure	*U*, *J* (eV)	A_{1g}	E_{g1}	E_{g2}
$P6_3/mmc$	0.0, 0.0	0.67	0.16	0.16
	3.5, 0.7	0.45	0.29	0.27
$Cmc2_1$	0.0, 0.0	0.59	0.31	0.10
	3.5, 0.7	0.41	0.45	0.14

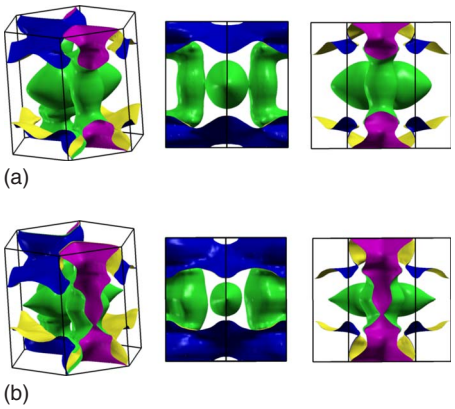

FIG. 8. (Color online) Comparison between (a) the LDA FS of orthorhombic $BaVS_3$ and (b) the corresponding QP FS derived from LDA+DMFT.

energy perspective, the (V1,V2) and (V3,V4) ions have similar characteristics, especially in the occupied part of the DOS. The A_{1g} occupation compared to the E_{g1} one is larger for the (V3,V4) ions. Because of the way of the shifts of the atomic positions in the monoclinic structure, it is not so surprising to find that already on an LDA level, the (V3,V4) and (V1,V2) ions appear to form somehow two different classes. Since the (V1,V2) ions are more isolated, the larger E_{g1} filling makes sense when being the more localized state. In spite of these differences, it is seen in Table V that the LDA crystal-field splitting within the t_{2g} manifold is greatly reduced in the CDW state. Note also that the spread of the A_{1g} WF is significantly enhanced in the LDA description of *Im* $BaVS_3$ (see Table VI).

D. LDA+DMFT study of the paramagnetic insulating regime

In order to overcome the obvious failure of LDA in describing the paramagnetic insulating state of $BaVS_3$, an

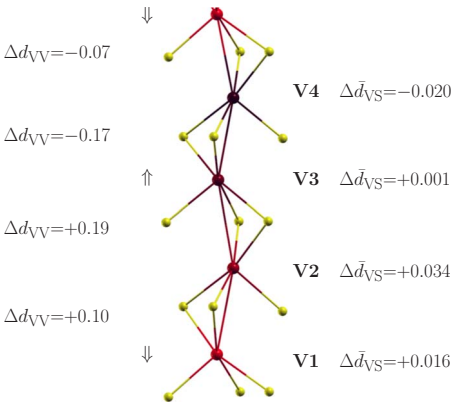

FIG. 9. (Color online) Single $BaVS_3$ chain for the monoclinic structure at 40 K. The numbers on the left mark the deviation of intrachain V-V distance in comparison to the value $d_{VV}=5.37$ a.u. in $Cmc2_1$ $BaVS_3$, whereas the numbers on the left denote the deviation of the average V-S distance. All values in are a.u. The arrows indicate the dominant shifts of the ions again with respect to the orthorhombic structure above the CDW instability.

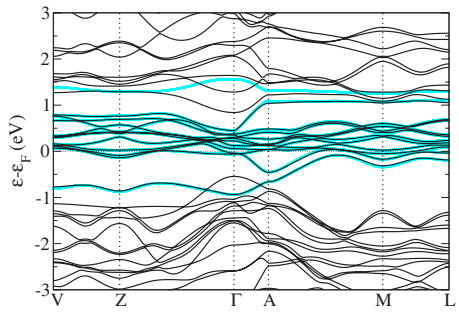

FIG. 10. (Color online) LDA band structure and derived t_{2g} Wannier bands (cyan/light gray) for monoclinic *Im* $BaVS_3$.

LDA+CDMFT approach was employed. Because of the revealed different behaviors of the inequivalent V ions already on the LDA level, the minimal cluster has to include all four V ions along the chain. Such a four-site cluster leads in the present case to the description within an effective 12-band model on the basis of the derived Wannier hamiltonian. The same values for U and J as for the metallic regime were used ($U=3.5$ eV, $J=0.7$ eV), no explicit interatomic Coulomb repulsion term was introduced. Due to the large computational effort for the QMC impurity solver, the lowest temperature with a still reasonable statistics we achieved was $T=460$ K.

Figure 12 exhibits the site- and orbital-resolved local spectral function obtained from CDMFT. It is seen that within this description, the system can be interpreted to be in a paramagnetic insulating state. The partially still remaining minor spectral weight at zero energy is due to the limitation concerning the handable temperature with the QMC solver. Remember that the experimental charge gap from precise optics measurements[19] equals only $\Delta_{ch}=0.42$ meV.

Obviously, the strong correlations lead to a substantial renormalization of the crystal-field splitting, since the E_g twofold is now widely separated in energy, shifting the E_{g2} state toward higher energy and somehow "out of the picture." The different tendencies in the character of the inequivalent V ions seen in LDA are now much more strongly enhanced. Thus, the (V1,V2) ions have now nearly exclusively E_{g1} weight, while the (V3,V4) ions show some mixed A_{1g}/E_{g1} occupation. This interesting result is also summa-

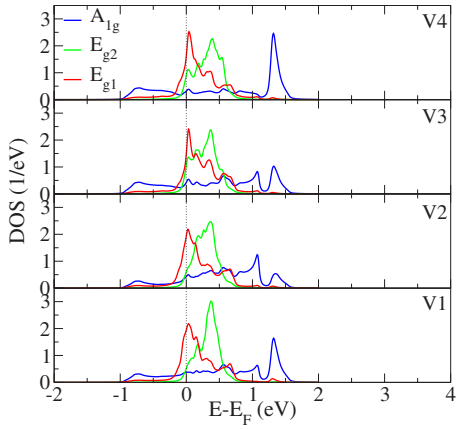

FIG. 11. (Color online) LDA DOS based on the derived t_{2g} Wannier functions for monoclinic *Im* $BaVS_3$.

TABLE V. On site terms of the t_{2g} Wannier Hamiltonian for *Im* $BaVS_3$ compared to the ones in the metallic phases. The values are in meV.

	V1	V2	V3	V4	$Cmc2_1$	$P6_3/mmc$
A_{1g}	478	473	460	477	423	395
E_{g1}	431	431	436	432	210	200
E_{g2}	448	444	443	448	236	200

rized in the site- and orbital-resolved occupations shown in Table VII. Hence, the charge transfer that was observed in the metallic regime due to strong correlations takes place also in the insulating state, now in a site-dependent manner. Whereas the (V1,V2) ions lose their A_{1g} occupation nearly completely and become orbitally polarized, the (V3,V4) ions fall more in the regime of orbital compensation, with the V4 ion gains some extra E_{g1} weight. On average, roughly speaking, the E_{g1} orbital is the winner of the CDW transition, since it replaces the A_{1g} orbital as the dominant orbital in the system. Concerning the question of charge order, the data do not provide a strong argument for either side. Albeit from the numbers there appears to be the slight tendency to put some minor extra charge on the (V1,V2) ions, due to the restrictions in quantitative accuracy of the formalism, this may be within the error bars. Remember that, experimentally, no charge order was found.[17]

The LDA+CDMFT method gives access to more quantities than solely the spectral functions and on site densities. To find out more about the nature of the CDW transition and the insulating state in $BaVS_3$, investigating the behavior of the self-energy $\mathbf{\Sigma}(i\omega_n)$ is very instructive. Note that in the present case, $\mathbf{\Sigma}$ corresponds to a 12×12 matrix, including information not only about on site but also intersite correlations within the four-site cluster.

It is seen in Fig. 13 that the on site self-energies for the various V ions display the expected behavior. While $\Sigma_{A_{1g}}$ and $\Sigma_{E_{g1}}$ have rather different amplitudes and zero-frequency slopes for (V1,V2), they scale similar for (V3,V4). The large negative increase of $\mathrm{Re}\,\Sigma_{E_{g1}}$ close to zero frequency for (V1,V2) leads to the strong shift of the QP spectral weight to lower energies observed in Fig. 12. An important qualitative finding is that none of the $Im\,\Sigma$ diverges at $\omega_n=0$. Hence, the opening of the gap in $BaVS_3$ is due to shifts of the QP states away from zero energy.

The inspection of the nearest-neighbor self-energy $\Sigma_{\text{V-V}}$ (see Fig. 14) reveals more details of the CDW state. For the (V3,V4) ions, $\mathrm{Re}\,\Sigma_{\text{V-V}}$ displays a salient increasing behavior when approaching zero frequency. Such a tendency for the intersite self-energy is a strong indication for the importance of intersite correlation effects leading to interatomic dimer formation.[35] However, within the crystal-field basis (derived from the LDA Hamiltonian), the occupation on (V3,V4) is of mixed (A_{1g},E_{g1}) character. Diagonalizing the interacting cluster Green's function may thus lead to an orbital basis which corresponds to this dimer symmetry. On the other hand, the V1-V2 pair does not show strong intersite correlations. Thus, these dominant E_{g1} occupied ions do not tend to form a spin singlet. It follows therefrom that the apparent spin gap in the insulating system is not originated from the direct correlated coupling of the neighboring E_{g1} spins on (V1-V2). However, one observes for the V2-V3 self-energies a minor tendency for singular behavior, especially for the E_{g1}-A_{1g} channel. One may conclude from this that the E_{g1} spins on (V1,V2) are somewhat effectively pinned by the neighboring dimers within the overall tetramerized state. This would explain the large drop in the magnetic susceptibility[4] and excess entropy[16] below the MIT.

It has to be noted that the intersite $\Sigma_{\text{V-V}}$ for V4-V1 is not a true pair self-energy as the others. Since the cellular DMFT approach we applied here breaks translational invariance, this special intersite self-energy connecting the surface of the cluster may not be obtained accurately. Thus, for completeness, we plotted in Fig. 14 instead $\Sigma_{\text{V1-V4}}$. The issue of translational-invariance breaking is surely a drawback of the used method. However, since the V4-V1 pair is expected to be in an intermediate state between V1-V2 and V3-V4, we believe that the qualitative result of how the V ions electronically relate to each other remains unchanged. Note that one option to restore the periodicity in the present context would have been to perform calculations in the chain-DMFT framework.[39] However, there, the different treatments of inter- and intrachain hoppings might cause other problems for $BaVS_3$, since the 1D character (as stated) is not very strongly indicated from the band Hamiltonian.

IV. SUMMARY AND CONCLUSIONS

The puzzling physics of $BaVS_3$ is dominated by the competition between the more itinerant A_{1g} state and the quasilo-

TABLE VI. Spread $\langle r^2\rangle$ of the t_{2g} WFs for *Im* $BaVS_3$ compared to the ones in the metallic phases. The values are in (a.u.^2).

	V1	V2	V3	V4	$Cmc2_1$	$P6_3/mmc$
A_{1g}	22.72	21.13	22.18	23.69	16.60	18.62
E_{g1}	17.61	18.04	18.39	17.54	17.55	17.10
E_{g2}	18.86	19.31	17.91	18.21	17.53	17.10

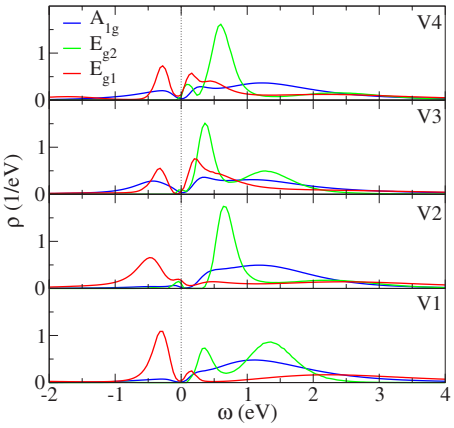

FIG. 12. (Color online) Local spectral functions from LDA+CDMFT for monoclinic *Im* $BaVS_3$. The QMC solver was used at $T=460$ K.

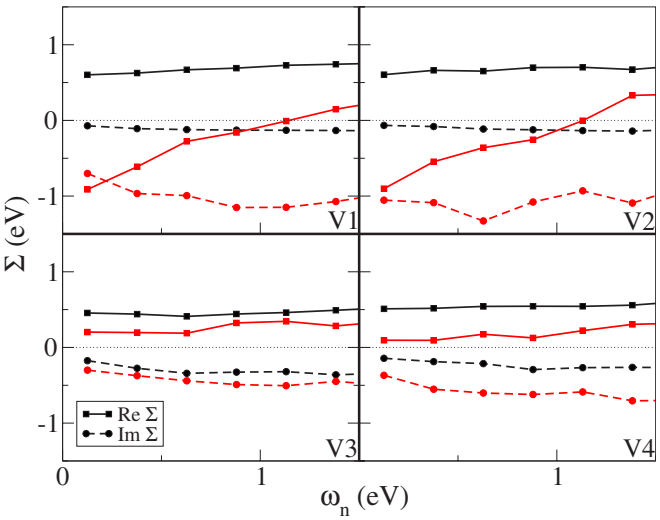

FIG. 13. (Color online) A_{1g} and E_{g1} on site self-energy $\Sigma(i\omega_n)$ for the four inequivalent V ions in monoclinic *Im* $BaVS_3$ at $T=460$ K. Dark lines correspond to A_{1g} and red (gray) lines to E_{g1}.

calized E_g states, which form together the t_{2g} manifold of the V($3d$) shell. Some theoretical models in the early days tried to rule out one or the other of those orbital sectors for playing an essential role. However, several recent experimental and theoretical studies revealed clearly the importance of the existence of both orbital types in order to find a way to understand the complex electronic phases of this system. Thus, $BaVS_3$ appears to be a manifest multiorbital system, and if at all, some orbital degrees of freedom might just freeze-out at very low temperatures.

LDA approaches to the electronic structure of $BaVS_3$ tend quite naturally to overestimate the itinerant character of the system. The A_{1g} associated Wannier orbital has an LDA filling of around 70% for the RT hexagonal structure, while the inclusion of strong electronic correlations within LDA+DMFT reduce this filling to about 50%. This is because a dominant A_{1g} filling becomes just too costly in the presence of reasonable mutual Coulomb interactions between the electrons. The balanced occupation of A_{1g} and E_g seems to be stable when going to the orthorhombic structure below T_S, yet the LDA+DMFT calculations revealed some tendency towards increasing the E_g filling even more. Note, however, that there is still some arbitrariness in what one calls an A_{1g}/E_g *orbital*, especially in the metallic regime and between different phases, and hence some margin in the derived numbers. Nonetheless, it was shown that in the paramagnetic insulating phase with the monoclinic structure, the average E_g occupation finally reaches about 70%.

The E_g states show a low QP coherence temperature and are expected to be effectively localized for elevated temperatures in the metal. Though the LDA approach (even when extended by linear expansions of the DMFT self-energy[14]) shows E_g FS sheets, it is very likely that the E_g QPs do not participate in the true Fermi surface in a well-defined manner. Hence, due to the rather large difference in the coherence temperatures, one may describe $BaVS_3$ to be in an effective orbital-selective insulating regime. As there is substantial hybridization between A_{1g} and E_{g1} below T_S, the low metallicity of $BaVS_3$, and especially the bad-metal regime below 150 K, may result from the scattering processes for the (quasi)itinerant electrons. The origin of the hexagonal-to-orthorhombic transition appears to be closely related to the A_{1g}-E_{g1} hybridization. It was shown that the E_{g1} Wannier orbital connects to two S2 ions, while the E_{g2} one hybridizes with only one apical S1 ion. It is likely that this imbalance favors the susceptibility for growing symmetry-breaking A_{1g}-E_{g1} hopping. Thereby, the large DOS close to the Fermi level is partly reduced when lifting the E_g degeneracy, and this driving force leads via the final zigzag intrachain distortion to a new energetic minimum. Albeit many details of the MIT are still open, as discussed in Ref. 14, the correlation-induced flattened A_{1g} FS sheets away from the high-symmetry directions in the BZ are good candidates for a meaningful matching with experimental findings.[13] Further experimental studies of the low-energy regime close to the MIT are needed to uncover more details.

TABLE VII. Orbital-resolved fillings for *Im* $BaVS_3$ from LDA+CDMFT within the crystal-field Wannier basis. The values in the left column correspond to the LDA result, while in the right column, the values for $U=3.5$ eV, $J=0.7$ eV (with $T=460$ K in the QMC impurity solver) are given.

	V1		V2		V3		V4		$\bar{V}$	
A_{1g}	0.49	0.12	0.40	0.11	0.62	0.47	0.61	0.34	0.53	0.26
E_{g1}	0.46	0.89	0.44	0.85	0.28	0.46	0.37	0.62	0.39	0.70
E_{g2}	0.05	0.03	0.07	0.07	0.11	0.03	0.10	0.02	0.08	0.03
Sum	1.00	1.04	0.91	1.03	1.01	0.96	1.08	0.98		

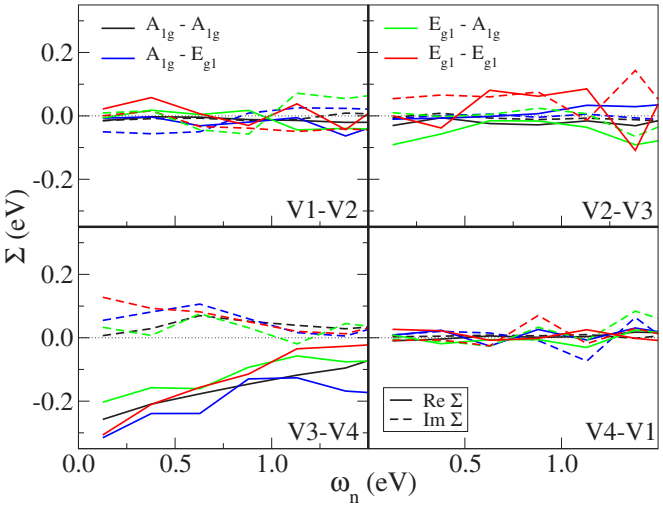

FIG. 14. (Color online) Intersite self-energy $\Sigma_{\text{V-V}}(i\omega_n)$ for the nearest-neighbor V-V pairs in monoclinic *Im* $BaVS_3$ at T=460 K. Note that the shown $\Sigma_{\text{V4-V1}}$ is not a true pair self-energy here (see text).

We revealed with LDA+CDMFT calculations that the insulating CDW state does not stay behind in terms of complexity of the electronic structure in comparison with the metallic regime. The tetramerization of the V ions, structurally an effective trimerization, leads to a quite different behavior. While the (V3,V4) pair apparently forms a correlated dimer with mixed A_{1g}/E_{g1} occupation, the (V1,V2) ions are strongly orbitally polarized with major E_{g1} occupation and negligible coupling. Note, however, that this picture is of course basis dependent, and we worked always in the Wannier basis derived from the LDA Hamiltonian. Hence, a new orbital basis may be found in the interacting regime where, e.g., the occupation for (V3,V4) has also polarized character. Concerning the "free" spins on (V1,V2), note that they are still coupled to the neighboring dimers, whereby their degrees of freedom are substantially reduced. The latter effect may serve as an explanation of the quenched local moments observed below T_{MIT}. Fagot *et al.*[17] proposed from anomalous x-ray measurements a dominant E_{g1} occupation on V1 and an additional dominant occupation of A_{1g} on V3, as well as no definite preferential occupation on (V2,V4). This would describe an orbital order modulated with $2c$ along the chain. Our picture differs by the fact that we do not find a dominant A_{1g} occupation but rather *two* ions, i.e., (V1,V2), with dominant E_{g1} weight. Although, from a local structural point of view the former proposition appears meaningful, the intersite correlation effects appear efficient in singling out dimer and isolated behavior. Note that dimer formation and nearest-neighbor spins may also be energetically favorable, since the former brings in some residual hopping whereas the latter yields energy from spin exchange. Recently, Fazekas *et al.*[40] proposed a minimal one-dimensional model, expecting thereby also nearest-neighbor E_g spins. However, the orbital degeneracy of the E_g multiplet, ascribed to spin-orbit coupling, was kept in that model.

The aspect of the spin degree of freedom in $BaVS_3$ was so far only scarcely discussed. Albeit it is expected that the former is an important ingredient in the understanding of the physics, its role in the different phases is still quite open. Nakamura *et al.*[18] reported anomalies in the temperature derivative of the magnetic susceptibility not only at T_{MIT} but also at the onset of the bad-metal regime ($\sim$160 K). Hence, the detailed role of the local E_g spins in the metal still poses important questions. Our study of the insulator renders it difficult to make precise statements about possible long-range order effects for the spin and orbitals, thus leaving questions concerning the classification of the electronic phase open. Furthermore, the mechanisms in conjunction with the famous magnetic transition at T_X need to be addressed. LDA+(C)DMFT computations may still help in delivering some further information associated with those problems, for instance, the calculation of magnetic susceptibilities in the insulating regime and the study of exchange interactions, as well as the investigation of the influence of the interchain coupling especially on the spin arrangement. More sophisticated model studies for multiorbital chains, perhaps with therefore well-adapted theoretical tools such as density matrix renormalization group,[41] may also deliver important new insights.

ACKNOWLEDGMENTS

We are indebted to A. Poteryaev, M. Posternak, A. Yamasaki, and O. K. Andersen, as well as S. Fagot, P. Foury-Leylekian, J.-P. Pouget, and S. Ravy, for useful discussions and remarks. This work has been supported by the European Union (under contract "Psi-k f-electrons," HPRN-CT-2002-00295), CNRS, and Ecole Polytechnique. Financial support was provided by the "Psi-k *f*-electron" Network under Contract No. HPRN-CT-2002-00295. Computations were performed at IDRIS Orsay.

[1] R. Gardner, M. Vlasse, and A. Wold, Acta Crystallogr., Sect. B: Struct. Crystallogr. Cryst. Chem. **B25**, 781 (1969).
[2] O. Massenet, J. Since, J. Mercier, M. Avignon, R. Buder, and V. Nguyen, J. Phys. Chem. Solids **40**, 573 (1979).
[3] K. Matsuura, T. Wada, T. Nakamizo, H. Yamauchi, and S. Tanaka, Phys. Rev. B **43**, 13118 (1991).
[4] T. Graf, D. Mandrus, J. M. Lawrence, J. D. Thompson, P. C. Canfield, S.-W. Cheong, and L. W. Rupp, Phys. Rev. B **51**, 2037 (1995).
[5] C. H. Booth, E. Figueroa, J. M. Lawrence, M. F. Hundley, and J. D. Thompson, Phys. Rev. B **60**, 14852 (1999).
[6] M.-H. Whangbo, H.-J. Koo, D. Dai, and A. Villesuzanne, J. Solid State Chem. **175**, 384 (2003).
[7] T. Inami, K. Ohwada, H. Kimura, M. Watanabe, Y. Noda, H. Nakamura, T. Yamasaki, M. Shiga, N. Ikeda, and Y. Murakami, Phys. Rev. B **66**, 073108 (2002).

[8] S. Fagot, P. Foury-Leylekian, S. Ravy, J.-P. Pouget, M. Anne, G. Popov, M. V. Lobanov, and M. Greenblatt, Solid State Sci. **7**, 718 (2005).
[9] H. Nakamura, T. Yamasaki, S. Giri, H. Imai, M. Shiga, K. Kojima, M. Nishi, and K. K. N. Metoki, J. Phys. Soc. Jpn. **69**, 2763 (2000).
[10] W. Higemoto, A. Koda, G. Maruta, K. Nishiyama, H. Nakamura, S. Giri, and M. Shiga, J. Phys. Soc. Jpn. **71**, 2361 (2002).
[11] L. Forró, R. Gaál, H. Berger, P. Fazekas, K. Penc, I. Kézsmárki, and G. Mihály, Phys. Rev. Lett. **85**, 1938 (2000).
[12] N. Barisić, I. Kézsmárki, P. Fazekas, G. Mihály, H. Berger, L. Demkó, and L. Forró, arXiv:cond-mat/0602262 (unpublished).
[13] S. Fagot, P. Foury-Leylekian, S. Ravy, J.-P. Pouget, and H. Berger, Phys. Rev. Lett. **90**, 196401 (2003).
[14] F. Lechermann, A. Georges, A. Poteryaev, S. Biermann, M. Posternak, A. Yamasaki, and O. K. Andersen, Phys. Rev. B **74**, 125120 (2006).
[15] G. Mihály, I. Kézsmárki, F. Zámborszky, M. Miljak, K. Penc, P. Fazekas, H. Berger, and L. Forró, Phys. Rev. B **61**, R7831 (2000).
[16] H. Imai, H. Wada, and M. Shiga, J. Phys. Soc. Jpn. **65**, 3460 (1996).
[17] S. Fagot, P. Foury-Leylekian, S. Ravy, J.-P. Pouget, E. Lorenzo, Y. Joly, M. Greenblatt, M. V. Lobanov, and G. Popov, Phys. Rev. B **73**, 033102 (2006).
[18] M. Nakamura, A. Sekiyama, H. Namatame, A. Fujimori, H. Yoshihara, T. Ohtani, A. Misu, and M. Takano, Phys. Rev. B **49**, 16191 (1994).
[19] I. Kézsmárki, G. Mihály, R. Gaál, N. Barišić, A. Akrap, H. Berger, L. Forró, C. C. Homes, and L. Mihály, Phys. Rev. Lett. **96**, 186402 (2006).
[20] H. Nakamura, H. Imai, and M. Shiga, Phys. Rev. Lett. **79**, 3779 (1997).
[21] J. Málek, S.-L. Drechsler, S. Flach, E. Jeckelmann, and K. Kladko, J. Phys. Soc. Jpn. **72**, 2277 (2003).
[22] F. Lechermann, S. Biermann, and A. Georges, Phys. Rev. Lett. **94**, 166402 (2005).
[23] V. I. Anisimov, A. I. Poteryaev, M. A. Korotin, A. O. Anokhin, and G. Kotliar, J. Phys.: Condens. Matter **9**, 7359 (1997).
[24] A. I. Lichtenstein and M. I. Katsnelson, Phys. Rev. B **57**, 6884 (1998).
[25] B. Meyer, C. Elsässer, F. Lechermann, and M. Fähnle, FORTRAN 90 Program for Mixed-Basis-Pseudopotential Calculations for Crystals, Max-Planck-Institut für Metallforschung, Stuttgart (unpublished).
[26] N. Marzari and D. Vanderbilt, Phys. Rev. B **56**, 12847 (1997).
[27] I. Souza, N. Marzari, and D. Vanderbilt, Phys. Rev. B **65**, 035109 (2001).
[28] C. Castellani, C. R. Natoli, and J. Ranninger, Phys. Rev. B **18**, 4945 (1978).
[29] R. Frésard and G. Kotliar, Phys. Rev. B **56**, 12909 (1997).
[30] J. E. Hirsch and R. M. Fye, Phys. Rev. Lett. **56**, 2521 (1986).
[31] G. Biroli, O. Parcollet, and G. Kotliar, Phys. Rev. B **69**, 205108 (2004).
[32] T. Maier, M. Jarrell, T. Pruschke, and M. H. Hettler, Rev. Mod. Phys. **77**, 1027 (2005).
[33] A. Lichtenstein, M. Katsnelson, and G. Kotliar, in *Electron Correlations and Materials Properties*, 2nd ed., edited by A. Gonis (Kluwer, New York, in press).
[34] A. I. Poteryaev, A. I. Lichtenstein, and G. Kotliar, Phys. Rev. Lett. **93**, 086401 (2004).
[35] S. Biermann, A. Poteryaev, A. I. Lichtenstein, and A. Georges, Phys. Rev. Lett. **94**, 026404 (2005).
[36] M. Ghedira, M. Anne, J. Chenavas, M. Marezio, and F. Sayetat, J. Phys. C **19**, 6489 (1986).
[37] L. Mattheiss, Solid State Commun. **93**, 791 (1995).
[38] M.-H. Whangbo, H.-J. Koo, D. Dai, and A. Villesuzanne, J. Solid State Chem. **165**, 345 (2002).
[39] S. Biermann, A. Georges, A. Lichtenstein, and T. Giamarchi, Phys. Rev. Lett. **87**, 276405 (2001).
[40] P. Fazekas *et al.*, J. Magn. Magn. Mater. **310**, 928 (2007).
[41] S. R. White, Phys. Rev. Lett. **69**, 2863 (1992).